Molecular Therapy
Nucleic Acids
Original Article

Inhibition of microRNA-30a alleviates vascular remodeling in pulmonary arterial hypertension

Wenrui Ma,[1,2,3,4] Zhihua Qiu,[1,2,3,4] Zeyang Bai,[1,2,3,4] Yong Dai,[1,2,3] Chang Li,[1,2,3] Xiao Chen,[1,2,3] Xiaoxiao Song,[1,2,3] Dingyang Shi,[1,2,3] Yanzhao Zhou,[1,2,3] Yajie Pan,[1,2,3] Yuhua Liao,[1,2,3] Mengyang Liao,[1,2,3] and Zihua Zhou[1,2,3]

[1]Department of Cardiology, Union Hospital, Tongji Medical College, Huazhong University of Science and Technology, Wuhan 430022, China; [2]Institute of Cardiology, Union Hospital, Tongji Medical College, Huazhong University of Science and Technology, Wuhan 430022, China; [3]Key Lab of Molecular Biological Targeted Therapies of the Ministry of Education, Union Hospital, Tongji Medical College, Huazhong University of Science and Technology, Wuhan 430022, China

The excessive and ectopic pulmonary artery smooth muscle cells (PASMCs) are crucial to the pathogenesis of pulmonary arteriole (PA) remodeling in pulmonary arterial hypertension (PAH). We previously found that microRNA (miR)-30a was significantly increased in acute myocardial infarction (AMI) patients and animals, as well as in cultured cardiomyocytes after hypoxia, suggesting that it might be strongly associated with hypoxia-related diseases. Here, we investigated the role of miR-30a in the PASMC remodeling of PAH. The expression of miR-30a was higher in the serum of PAH patients compared with healthy controls. miR-30a was mainly expressed in PAs and was increased in PASMCs after hypoxia, mediating the downregulation of p53 tumor suppressor protein (P53). Genetic knockout of miR-30a effectively decreased right ventricular (RV) systolic pressure (RVSP), PA, and RV remodeling in the Su5416/hypoxia-induced and monocrotaline (MCT)-induced PAH animals. Additionally, pharmacological inhibition of miR-30a via intratracheal liquid instillation (IT-L) delivery strategy showed high efficiency, which downregulated miR-30a to mitigate disease phenotype in the Su5416/hypoxia-induced PAH animals, and these beneficial effects could be partially reduced by simultaneous P53 inhibition. We demonstrate that inhibition of miR-30a could ameliorate experimental PAH through the miR-30a/P53 signaling pathway, and the IT-L delivery strategy shows good therapeutic outcomes, providing a novel and promising approach for the treatment of PAH.

INTRODUCTION

Pulmonary arterial hypertension (PAH) is a devastating disease characterized by progressive pulmonary arteriole (PA) remodeling, leading to an increasing right ventricular (RV) afterload and ultimately death.[1] During the past 20 years, the treatment of PAH has achieved great progress, especially with the application of targeted drugs.[2] However, these current treatments are limited to vasoconstriction, which plays a role in approximately 5% of PAH patients and hardly reverses remodeling vessels.[1] In fact, the critical mechanism of vascular remodeling is excessive and ectopic smooth muscle cells (SMCs), which are directly involved in thickening the media and migrating to muscularize distal vessels.[3] Moreover, studies have shown that SMCs, not endothelium, are selected as a source of cells to establish the neointima to occlude the arterioles.[4] Therefore, it is of great significance to explore a novel approach to prevent SMC remodeling in treating PAH.

MicroRNAs (miRNAs, miRs) are noncoding small RNAs with a length of approximately 22 nt, which negatively modulate target coding mRNAs by either repressing translation or degrading mRNA.[5] A growing number of studies have shown that miRNAs are widely involved in the physiological and pathological processes of PAH.[6,7] miR-30a was first found to regulate the expression of brain-derived neurotrophic factors in the prefrontal cortex,[8] and it was subsequently found to be involved in tumor progression through different mechanisms.[9] Studies have shown that miR-30a is dysregulated in multiple cancer diseases, including lung cancer, breast cancer, and hepatocyte carcinoma, affecting cell proliferation.[10] PAH and cancer share some of the same characteristics, one of which is excessive cell proliferation leading to structural changes in blood vessels,[11] which indicates that miR-30a may be associated with the vascular remodeling of PAH. At present, there are few reports on the role of miR-30a in PAH, and their conclusions are controversial. Researchers have shown that miR-30a is decreased in the microarrays of endoarterial biopsy, speculating that it may be related to pulmonary artery endothelial cells (PAECs), but miR-30a is increased in the serum of PAH patients.[12,13] Therefore, the relationship between miR-30a and PAH is not clear, does not involve remodeling pulmonary artery SMCs (PASMCs), and remains to be clarified.

In our previous study, we found that miR-30a was significantly increased in the serum of acute myocardial infarction (AMI) patients

Received 16 November 2020; accepted 9 September 2021;
https://doi.org/10.1016/j.omtn.2021.09.007.

[4]These authors contributed equally

Correspondence: Zihua Zhou, PhD, Department of Cardiology, Union Hospital, Tongji Medical College, Huazhong University of Science and Technology, 1277 Jiefang Avenue, Wuhan 430022, China.
E-mail: zzhua2001@163.com
Correspondence: Mengyang Liao, PhD, Department of Cardiology, Union Hospital, Tongji Medical College, Huazhong University of Science and Technology, 1277 Jiefang Avenue, Wuhan 430022, China.
E-mail: liaomengyang87@163.com

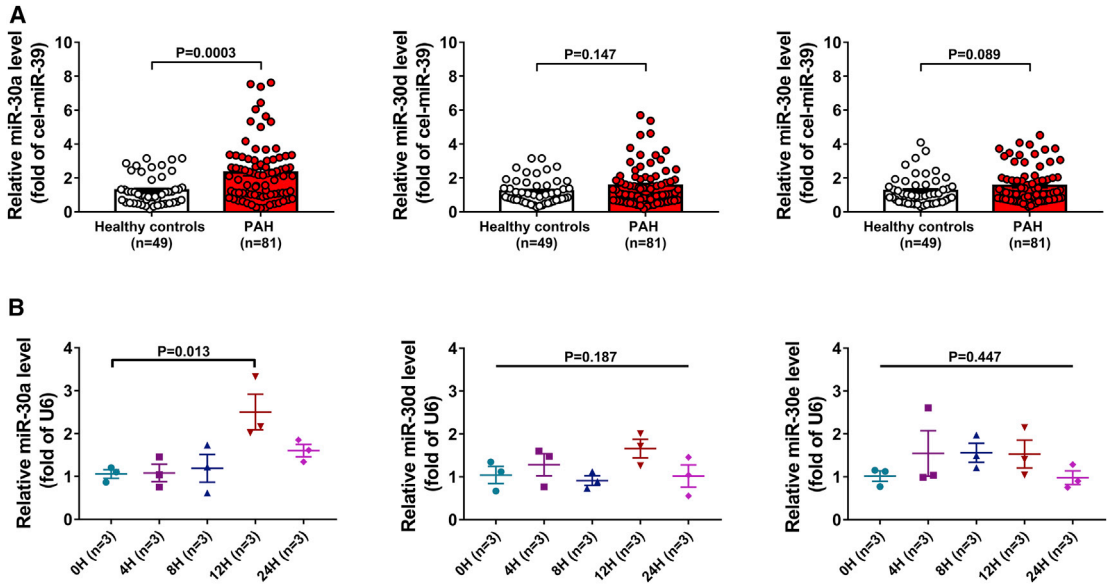

Figure 1. miR-30a is increased in PAH patients and PASMCs after hypoxia

(A) Expression levels of miR-30a/d/e in the serum of PAH patients and healthy controls detected by qRT-PCR. The relative quantification of qRT-PCR products was normalized against cel-miR-39 expression, and the miR-30a/d/e levels in the serum of PAH patients were relative to those in the serum of healthy controls. (B) Expression levels of miR-30a/d/e in PASMCs exposed to 1% hypoxia condition detected by qRT-PCR. The relative quantification of qRT-PCR products was normalized against U6 expression, and the quantifications of miR-30a/d/e levels were relative to the control group. Data are expressed as means ± SEM. The Mann-Whitney U test was used for the comparison between two groups in (A). The one-way analysis of variance was used for the comparison among multiple groups, followed by a Bonferroni's post hoc test in (B). $p < 0.05$ was considered as statistically significant.

and animals *in vivo*, as well as in cultured cardiomyocytes after hypoxic stimulation *in vitro*, and it deteriorated cardiac function by inhibiting autophagy activities.[14] Similarly, hypoxia is the key trigger mechanism of the vascular remodeling of PAH,[15] and changes in the level of miR-30a may also be involved in the remodeling of PASMCs. This study focuses on the changes of miR-30a in PAH patients, PAH animals, and PASMCs after hypoxia. The effects on PAs and RV remodeling were also evaluated by genetic and pharmacological inhibition of miR-30a in the Su5416/hypoxia-induced and monocrotaline (MCT)-induced PAH animals. Moreover, intratracheal liquid instillation (IT-L) of a miR-30a inhibitor was used to explore a novel delivery strategy for PAH treatment.

RESULTS

miR-30a is increased in PAH patients, PAs, and PASMCs after hypoxia

First, we sought to explore the expression levels of the miR-30 family (miR-30a, miR-30b, miR-30c, miR-30d, miR-30e) in the serum of PAH patients compared to those in healthy controls. We observed a higher expression of miR-30a, miR-30d, and miR-30e in PAH patients, among which the level of miR-30a was the most strongly expressed subtype (Figure 1A). There was no significant change in the expression levels of miR-30b and miR-30c in PAH patients compared to those in healthy controls (Figure S2A). The clinical characteristics of the patients are shown in Table 1. To validate these observations, we analyzed the expression levels of the miR-30 family in PASMCs at different time points under hypoxic conditions. We observed that the most significant change in the miR-30 family cluster was miR-30a (Figure 1B), rather than other members of this family (Figure S2B), which was consistent with our previous findings.[14] Then, we examined the expression levels of miR-30a in the RV, lung tissues, and PAs in PAH animals. We first confirmed the isolated PAs (mainly PASMCs) and whole-lung tissue (mainly PAECs) by western blot analysis (Figure S2C) as reported.[16] As shown in Figure S2D, there was an increasing expression of miR-30a in PAs rather than in other tissues in the Su5416/hypoxia-induced mice. These data suggested that miR-30a may play a potential role in PASMCs and PAH.

Although p53 tumor suppressor protein (P53) is the most well-known target gene of miR-30a,[17] it is still unknown whether this target can be modulated by miR-30a in PASMCs (Figure S3A). To test this hypothesis, PASMCs were exposed to hypoxic conditions (1% O_2) at different time points. The analysis of RNA revealed a significant increase in miR-30a after hypoxia for 12 h (Figure S3B). The expression of hypoxia inducible factor (HIF)-1α was increased while the expression of P53 was decreased at the same time point by the analysis of protein (Figure S3C). These indicated that the increasing expression level of miR-30a might lead to a decrease in gene expression of P53. Consequently, the effects of miR-30a inhibitors and mimics were observed to investigate this possibility by the analysis of RNA (Figure S3D). As expected, the expression of P53 could be significantly upregulated by miR-30a inhibitors and downregulated

Table 1. Clinical characteristics of PAH patients and healthy controls

	Control (n = 49)	PAH (n = 81)
Sex (female, n (%))	23 (46.9%)	37 (45.7%)
Age (years)	46.6 ± 11.4	54.3 ± 17.8
NYHA (n (%))		
I	–	5 (6.2%)
II	–	24 (29.6%)
III	–	39 (48.2%)
IV	–	13 (16%)
EF (%)	–	48.28 ± 15.64
TRV (m/s)	–	3.32 ± 0.60
PA (cm)	–	3.15 ± 0.48
sPAP (mmHg)	–	53.78 ± 18.94
miR-30a	1.26 ± 0.87	2.32 ± 1.75
Smoking (n (%))	–	22 (27.2%)
Comorbidities (n (%))		
Diabetes mellitus	–	14 (17.3%)
Hyperlipidemia	–	26 (32.1%)
CAD	–	32 (39.5%)
COPD	–	10 (12.3%)
Atrial fibrillation	–	13 (16%)
Medication (n (%))		
Anticoagulant agents	–	57 (70.4%)
Lipid-lowering medications	–	43 (53.1%)
CCBs	–	21 (25.9%)
Beta blockers	–	60 (74.1%)
ACE inhibitors	–	10 (12.3%)
ARBs	–	45 (55.6%)
Diuretic agents	–	45 (55.6%)
ERAs	–	9 (11.1%)
PDE5 inhibitors	–	3 (3.7%)
Prostacyclins	–	8 (9.9%)
Lab investigation parameters		
BNP (pg/mL)	–	889.07 ± 1,007.99
TC (mmol/L)	–	3.62 ± 0.97
TGs (mmol/L)	–	1.33 ± 0.82
LDL (mmol/L)	–	2.26 ± 0.77
HDL (mmol/L)	–	1.04 ± 0.39
Cr (μmol/L)	–	100.27 ± 61.33
BUN (mmol/L)	–	7.45 ± 4.56
ALT (U/L)	–	39.95 ± 39.50
AST (U/L)	–	36.37 ± 31.28
FG (mmol/L)	–	5.14 ± 1.41
Hb (g/L)	–	127.57 ± 24.22

NYHA, cardiac function classification from New York Heart Association; EF, ejection fraction; TRV, peak tricuspid regurgitation velocity; PA, pulmonary artery diameter; sPAP, systolic pulmonary artery pressure; CAD, coronary artery disease; COPD, chronic obstructive pulmonary disease; CCB, calcium-channel blocker; ACE, angiotensin-converting enzyme; ARB, angiotensin receptor blocker; ERA, endothelin receptor antagonist; PDE5, phosphodiesterase 5; BNP, brain natriuretic peptide; TC, total cholesterol; TG. triglyceride; LDL, low-density lipoprotein; HDL, high-density lipoprotein; Cr, creatinine; BUN, blood urea nitrogen; ALT, alanine aminotransferase; AST, aspartate aminotransferase; FG, fasting blood glucose; Hb, hemoglobin.

by miR-30a mimics by the analysis of protein (Figure S3E). All data confirmed that P53 was a target gene of miR-30a in PASMCs.

Knockout of miR-30a alleviates RV systolic pressure (RVSP) and RV hypertrophy in the Su5416/hypoxia mouse model

In order to evaluate the role of miR-30a in the pathogenesis of PAH directly, miR-30a knockout (KO) and wild-type (WT) mice were prepared to establish the Su5416 (Su)/hypoxia (Hx) mouse model. The results indicated that there was an increase in RVSP in the WT+Hx/Su and miR-30a KO+Hx/Su groups compared with that in the WT+Nor (normoxia)/Veh (vehicle) and miR-30a KO+Nor/Veh groups (Figure 2A). Additionally, RVSP in the miR-30a KO+Hx/Su group was remarkably decreased compared with that in the WT+Hx/Su group, which implied that miR-30a is directly involved in the pathogenesis of PAH (Figure 2A). No obvious difference was found among the WT+Nor/Veh and miR-30a KO+Nor/Veh groups. Representative images of RVSP are shown in Figure 2E.

Then, we investigated the remodeling of RV among the four groups. We found that the miR-30a KO+Hx/Su group exhibited significant reductions in RV/(left ventricular [LV]+ interventricular septum [S]), cross-sectional area (CSA) of myocardium, and myocardial fibrosis compared to those in the WT+Hx/Su group (Figures 2B–2D). These findings showed that deregulation of miR-30a was able to treat RV hypertrophy. In addition, we also found that miR-30a knockout clearly reduced the mRNA expression levels of markers related to myocardial fibrosis, including collagen I, transforming growth factor β (TGF-β), and Smad2 (Figure 2H). Representative images of hematoxylin and eosin (H&E) and Masson's trichrome staining of the RV are shown in Figures 2F and 2G.

Knockout of miR-30a activates apoptosis of PAs to prevent vascular remodeling in the Su5416/hypoxia mouse model

PAH is characterized by persistent vasoconstriction and progressive obstruction of pulmonary arteries through a process of intimal and medial thickening.[18] Thus, to assess the therapeutic effect of miR-30a knockout on proliferative vascular remodeling, the percentage of medial wall thickness (MT%), wall area (WA%), and the degree of muscularization of vessels were determined. Representative images of the pulmonary vascular remodeling are shown in Figure 3A. As illustrated in Figures 3C and 3D, compared with those in the WT+Nor/Veh group, the MT% and WA% of PAs in the WT+Hx/Su group were increased, and the miR-30a KO+Hx/Su group could clearly mitigate these changes in vascular remodeling. Moreover, the percentage of muscularized pulmonary vessels in the miR-30a KO+Hx/Su group was remarkably decreased compared with that in the WT+Hx/Su group (Figure 3E). No changes were

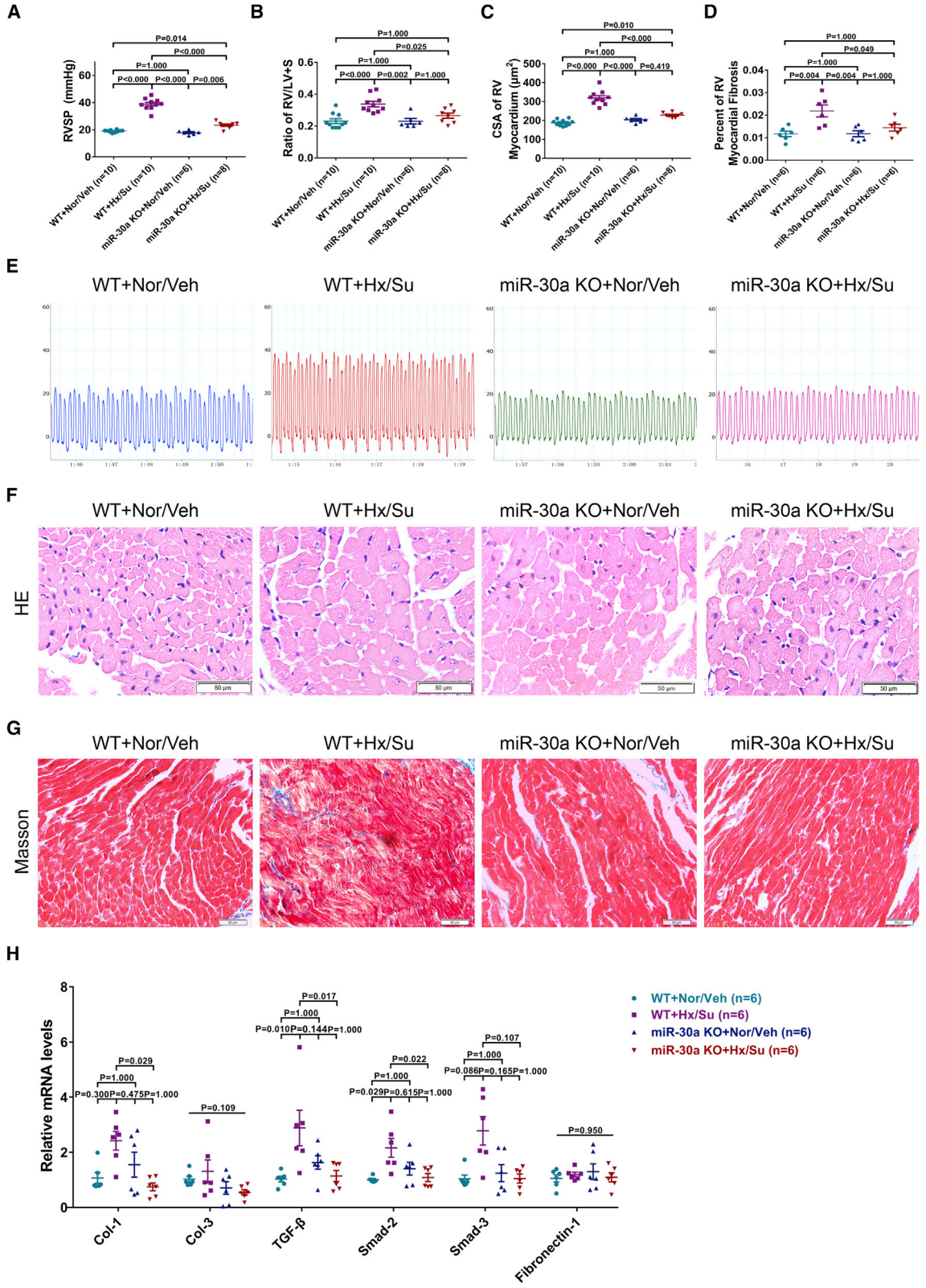

(legend on next page)

observed among the WT+Nor/Veh, miR-30a KO+Nor/Veh, and miR-30a KO+Hx/Su groups.

Then, we focused on the target molecules associated with the apoptosis of PAs. To detect the effect of miR-30a knockout on the apoptotic activities of PAs, a TUNEL (terminal deoxynucleotidyl transferase-mediated dUTP nick end labeling) assay was performed (Figure 3B). The results indicated that the number of TUNEL-positive PASMCs was much higher in the miR-30a KO+Hx/Su mice than in the WT+Hx/Su mice, suggesting that knockout of miR-30a would enhance apoptotic activities in PAs (Figure 3F). Further studies illustrated that the expression level of the target gene P53 as well as phosphorylated (P)-P53 was decreased in the WT+Hx/Su group, accompanied by lower expression of Bax/Bcl-2 and cleaved caspase-3/caspase-3, and it could be restored in the miR-30a KO+Hx/Su group (Figure 3G), which also demonstrated that inhibition of miR-30a could improve the antiapoptotic capacity of PAs.

Knockout of miR-30a attenuates RVSP, RV hypertrophy, and fibrosis in the MCT mouse model

To further verify the role of miR-30a in PAH, WT and miR-30a KO mice were treated with MCT to establish another PAH animal model. In the WT+MCT group, we found a significant increase in RVSP and RV/(LV+S) compared with those in the WT group, and the same results were observed in miR-30a KO mice (Figures 4A and 4B). Also, miR-30a KO mice showed lower RVSP and RV/(LV+S) than did WT mice when treated with MCT (Figures 4A and 4B). No obvious difference was observed between WT and miR-30a KO mice. Representative images of RVSP are shown in Figure 4E.

Similarly, RV hypertrophy and myocardial fibrosis were determined in all animals. The results revealed that there was a remarkable increase in the CSA of myocardium in the WT and miR-30a KO mice in response to MCT (Figure 4C). However, the CSA of myocardium in the miR-30a KO+MCT group was significantly decreased compared with that in the WT+MCT group (Figure 4C). Furthermore, WT mice showed more severe RV fibrosis, while miR-30a KO mice were able to mitigate that when treated with MCT (Figure 4D). No clear difference was observed between the WT and miR-30a KO groups in terms of RV hypertrophy and fibrosis. miR-30a knockout in the MCT PAH model also significantly decreased the mRNA expression levels of markers related to myocardial fibrosis, including collagen I, collagen III, and fibronectin-1 (Figure 4H). Representative images of H&E and Masson's trichrome staining of the RV are shown in Figures 4F and 4G.

Knockout of miR-30a enhances apoptosis of PAs to reverse vascular remodeling in the MCT mouse model

To test whether knockout of miR-30a could improve vascular reconstruction in the MCT PAH model, MT%, WA%, and the degree of muscularization of vessels were calculated. Representative images of the pulmonary vascular remodeling are shown in Figure 5A. As illustrated in Figures 5B and 5C, the MT% and WA% of PAs in the WT and miR-30a KO groups were increased when treated with MCT, but miR-30a KO mice had significantly less severe vascular remodeling than did WT mice. The results also showed that the ratio of muscularized PAs in WT animals was remarkably elevated compared with miR-30a KO animals in response to MCT (Figure 5D). No changes were observed among WT and miR-30a KO control mice.

We also evaluated the effect of miR-30a ablation on apoptosis of PAs. As illustrated in Figure 5E, the expression of P-P53, P53, Bax/Bcl-2, and cleaved caspase-3/caspase-3 was decreased in WT mice treated with MCT, whereas the protein expression of these was significantly elevated in miR-30a KO mice compared to that in WT mice. This implied that knockout of miR-30a could also upregulate the expression of P53 and P-P53, thereby activating the apoptotic activity of PAs to reverse the remodeling of PAs in the MCT-induced PAH model.

Intratracheal instillation of miR-30a antagomir reduces RVSP and RV hypertrophy in the Su5416/hypoxia mouse model

Drug delivery through the airways has been used to treat and prevent a growing number of respiratory diseases.[18] Studies have found that IT-L requires a smaller dose of drugs, has lower immunotoxicity, and has higher lung expression levels and tissue specificity than do intravenous and abdominal administration, making it one of the ideal methods for miRNA delivery.[19] Whether the curative effect against the development of PAH detected in miR-30a KO mice could be replaced by pharmacological inhibition of miR-30a remained to be tested. A schematic of the experimental design is illustrated in Figure S1C. We first confirmed that IT-L was an efficient delivery strategy that could clearly reduce the expression level of miR-30a in the lungs (Figure S4). The findings further revealed that RVSP and RV/(LV+S) in the Hx/Su and Hx/Su+anti-negative control (NC) groups were remarkably elevated compared with those in the control group, while they were decreased after treatment with miR-30a antagomir

Figure 2. Knockout of miR-30a alleviates RVSP and RV hypertrophy in the Su54116/hypoxia mouse model

(A) Assessment of right ventricular (RV) systolic pressure (RVSP) by right cardiac catheterization. (B) RV hypertrophy measured by the weight ratio of RV/(left ventricular [LV]+interventricular septum [S]). (C) Quantification of the RV cardiomyocytes cross-sectional area (CSA). (D) Quantification of the RV fibrotic area. (E) Representative images of RVSP in the four groups. (F) Representative images of hematoxylin and eosin (H&E) staining of the RV cardiomyocytes in the four groups. Scale bars, 50 μm. (G) Representative images of Masson's trichrome staining of the RV in the four groups. Scale bars, 50 μm. (H) mRNA expression levels of Col-1 (collagen I), Col-3 (collagen III), TGF-β (transforming growth factor β), Smad2 (SMAD family member 2), Smad3 (SMAD family member 3), and fibronectin-1 were analyzed by qRT-PCR. Data are expressed as means ± SEM. The experiment was repeated three times. A one-way ANOVA was used for the comparison among multiple groups, followed by Bonferroni's post hoc test in (A)–(D), and TGF-β of (H). The nonparametric data were analyzed using a Kruskal-Wallis test in Col-1, Col-3, Smad2, Smad3, and fibronectin-1 of (H). $p < 0.05$ was considered as statistically significant.

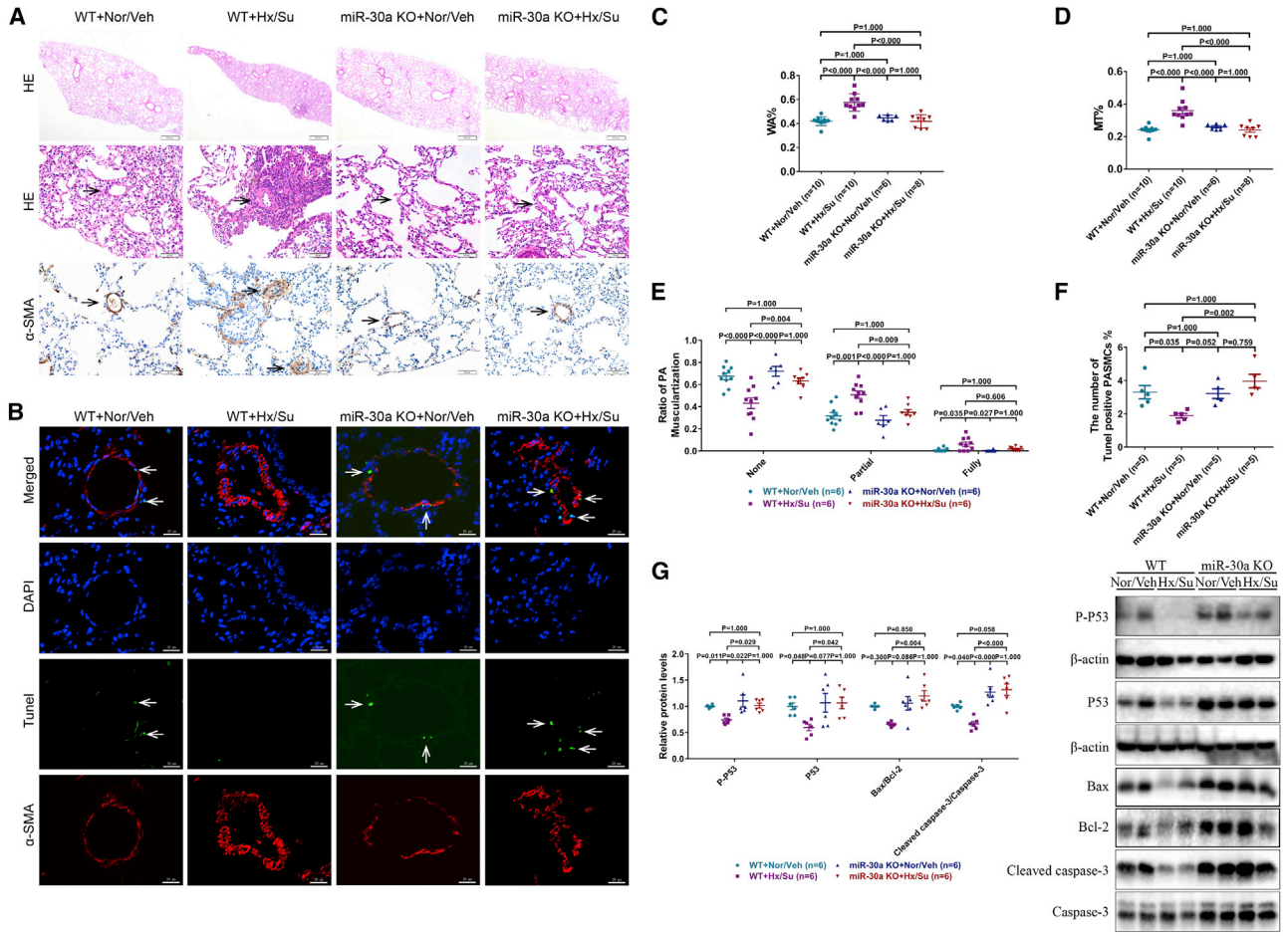

Figure 3. Knockout of miR-30a activates apoptosis of PAs to prevent vascular remodeling in the Su5416/hypoxia mouse model

(A) Representative images of the pulmonary arterioles (PAs) are provided from each group. Lung sections were stained with H&E (upper and middle panels) and α-smooth muscle actin (α-SMA, lower panel). Scale bars, 500 μm (upper panel) and 50 μm (middle and lower panels). (B) Representative images of TUNEL staining in the lung tissue from WT+Nor/Veh, WT+Hx/Su, miR-30a KO+Nor/Veh, and miR-30a KO+ Hx/Su mice. Staining of an anti-α-SMA antibody (red), TUNEL (green), and DAPI (blue) are presented. Scale bars, 20 μm. (C) Percentage wall area (WA%) of vessels. (D) Percentage medial wall thickness (MT%) of vessels. (E) Percentage of muscularized vessels. Each vessel was classified as either nonmuscular, partially muscular, or fully muscular as previously described. All the PAs (15–25 vessels per mouse, 25–75 μm in diameter) were calculated blinded to the source of the group. (F) Quantitation of the percentage of TUNEL-positive PASMCs per vessel (20–30 vessels per mouse, 25–75 μm in diameter). (G) The protein expression of P-P53, P53, Bax/Bcl-2, and cleaved caspase-3/caspase-3 of PAs. Data are expressed as means ± SEM. The experiment was repeated three times. A one-way ANOVA was used for the comparison among multiple groups, followed by a Bonferroni's post hoc test in (C) and (D), none and partial muscularization of (E), and cleaved caspase-3/caspase-3 of (G). The nonparametric data were analyzed using a Kruskal-Wallis test in full muscularization of (E) and P-P53, P53, and Bax/Bcl-2 of (G). $p < 0.05$ was considered as statistically significant.

(Figures 6A and 6B). Additionally, no changes were observed in control (Con) and Hx/Su+anti-miR-30a mice. Representative images of RVSP are shown in Figure 6E.

We next found that all of the mice showed an increased CSA of myocardium compared with control mice; however, mice treated with miR-30a antagomir exhibited a decreased CSA of myocardium compared with that in the Hx/Su and Hx/Su+anti-NC groups (Figure 6C). Additionally, miR-30a antagomir failed to mitigate the increased RV fibrosis (Figure 6D); however, it was able to decrease the mRNA expression levels of markers related to myocardial fibrosis, including collagen I, TGF-β, Smad2, and Smad3 (Figure 6H). Representative images of H&E and Masson's trichrome staining of the RV are shown in Figures 6F and 6G.

Intratracheal instillation of miR-30a antagomir increases apoptosis of PAs to mitigate vascular remodeling in the Su5416/hypoxia mouse model

To verify the protective effect of the inhibition of miR-30a, the MT%, WA%, and degree of muscularization of PAs were determined. Representative images of pulmonary vascular remodeling are shown in Figure 7A. As illustrated in Figures 7B and 7C, the MT% and WA% of

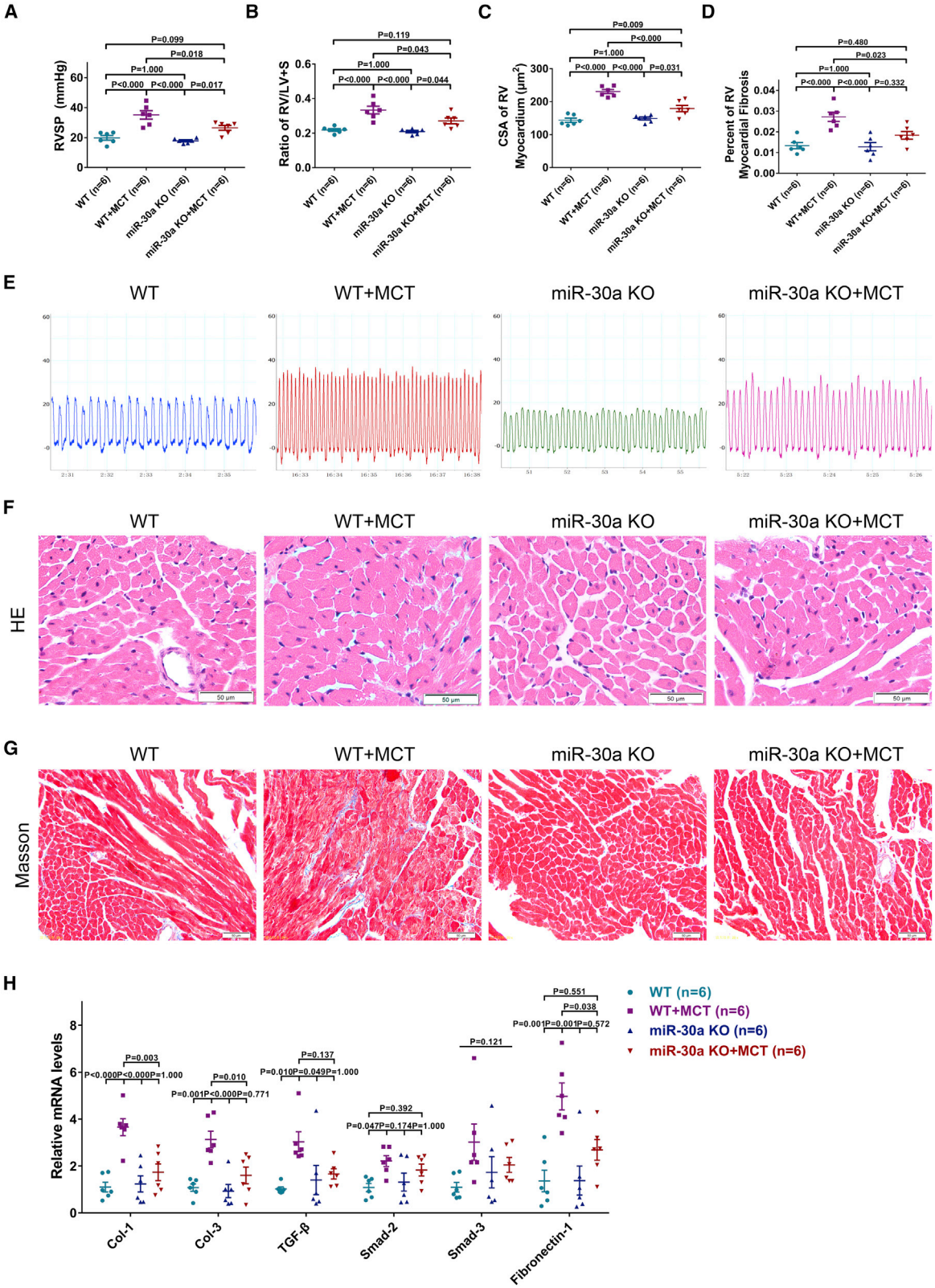

(legend on next page)

PAs in all of the groups were increased compared with those in the control group, and the Hx/Su+anti-miR-30a group attenuated these alterations in vascular remodeling. Histological analysis showed an obvious reduction in the percentage of muscularized PAs in the Hx/Su+anti-miR-30a group compared with those in the Hx/Su and Hx/Su+anti-NC groups (Figure 7D). No difference was found in the Hx/Su+anti-NC and Hx/Su+anti-miR-30a groups.

We then assessed the expression level of the target gene of PAs in mice treated with miR-30a antagomir. Western blot analysis showed that miR-30a antagomir could greatly increase the protein expression levels of P-P53, P53, Bax/Bcl-2, and cleaved caspase-3/caspase-3 in Su5416/hypoxia-induced mice (Figure 7E). To our surprise, mice treated with miR-30a antagomir exhibited even higher expression of P53 and P-P53 than did the control group (Figure 7E), suggesting that IT-L of miR-30a antagomir is an efficient delivery strategy for treating PAH.

Additionally, IT-L was used to deliver miR-30a antagomir as well as small interfering RNA (siRNA)-P53 , and siRNA-P53 with chemically modified was found to be more effective and stable in *in vivo* experiments.The results showed that RVSP, PAs, and RV remodeling were alleviated treated with miR-30a antagomir in the Su5416/hypoxia-induced mice, and these beneficial effects could be partially reduced by simultaneous P53 inhibition (Figures S6 and S7).

DISCUSSION

This study is the first to identify the role of miR-30a in PAH and describe its therapeutic effect by inhibition of miR-30a. We observed that the expression of miR-30a was increased in the serum of PAH patients, as well as in the PAs of PAH animals and PASMCs after hypoxia. Additionally, we revealed that miR-30a mediated the downregulation of P53 in PASMCs. Genetic deletion of miR-30a effectively reversed PA remodeling and increased RVSP and RV hypertrophy in the Su5416/hypoxia-induced and MCT-induced PAH animals. In addition, the IT-L delivery strategy showed high efficiency, which decreased miR-30a levels and attenuated the disease phenotype of PAH, and these beneficial effects could be partially reduced by simultaneous P53 inhibition.

The pathophysiology of PAH is heterogeneous and multifactorial, making the understanding of the pathogenesis of PAH challenging.[20] During the past few decades, miRNAs have emerged as crucial players in PAH.[21] Studies have shown that miR-98, miR-424, miR-503, miR-21, miR-130/301, miR-29b, and miR-125 are aberrantly expressed in PASMCs and PAECs and are involved in all of the processes of PAH.[22] The miR-30 family consists of five members, that is, miR-30a, miR-30b, miR-30c, miR-30d, and miR-30e. Although members of the miR-30 family share the same seed sequence and a similar set of targets, they perform differently in a variety of cells and tissues.[23] Recent studies have shown that miR-30a levels are decreased in PAECs but increased in the serum of PAH patients.[12,13] These contradictory findings led us to rethink the function of miR-30a in PAH. In fact, PASMCs, which work to thicken the media and formation of neointima,[4] as well as the muscularization of distal arterioles,[24] are the most promising target cells for vascular remodeling. However, the exact role of miR-30a in regulating the biological behavior of PASMCs in PAH remains unclear.

In this study, we first confirmed that miR-30a was the most strongly expressed subtype among miR-30 family members in the serum of PAH patients compared to those in healthy controls, which was consistent with our previous findings in AMI patients.[14] Then, we elucidated that miR-30a was relatively abundantly expressed in PAH patients (Figure S2E). Although this copy number analysis has some deficiencies in sensitivity and accuracy, which might be improved by RNA sequencing (RNA-seq) or microarrays in subsequent investigations, our results to some extent illustrated that the expression level of miR-30a could play functional effects in PAH. Moreover, our assay showed that the expression of miR-30a was increased in PAs of PAH mice and in PASMCs after hypoxia, suggesting that PASMCs could be the functional cells of miR-30a. Then, to explore the role of miR-30a in PAH animals, we constructed miR-30a knockout mice and established the Su5416/hypoxia and MCT PAH models. Results demonstrated that genetic knockout of miR-30a significantly alleviated RVSP, RV hypertrophy, fibrosis, and vascular remodeling in the two PAH models, but it had no effects on LV function and morphology (Figure S5). Thus, our findings indicated that genetic knockout of miR-30a could directly prevent PAH from progression.

The function of P53 as a major regulatory protein has been attributed to its involvement in cell proliferation, DNA repair, and cell cycle control.[25] In particular, P53 functions as both a sensitizer[26] and an activator[27] of apoptosis,[26] as well as in PAH. Researchers have shown that phosphorylation of P53 (Ser15, Ser20, Ser37, Ser46) modulates its activation to induce apoptosis through multiple effectors,[28,29] and it then upregulates the levels of the pro-apoptosis protein Bax whereas it downregulates the anti-apoptosis protein Bcl-2, activating caspase-9 and caspase-3 to induce apoptosis.[30] This P53-dependent apoptosis pathway contributes to vascular cells developing antiapoptotic and proliferative phenotypes, leading to intimal and medial thickening.[31] Meanwhile, P53 is one of the target genes of miR-30a involved in mitochondrial impairment and myocardial apoptosis.[17] In our study,

Figure 4. Knockout of miR-30a attenuates RVSP, RV hypertrophy, and fibrosis in the MCT mouse model

(A) Detection of RVSP by right cardiac catheterization. (B) RV hypertrophy measured by the weight ratio of RV/(LV+S). (C) Quantification of the CSA of RV cardiomyocytes. (D) Quantification of the RV fibrotic area. (E) Representative images of RVSP in the four groups. (F) Representative images of H&E staining of the RV cardiomyocytes in the four groups. Scale bars, 50 μm. (G) Representative images of Masson's trichrome staining of the RV in the four groups. Scale bars, 50 μm. (H) The mRNA expression levels of Col-1, Col-3, TGF-β, Smad2, Smad3, and fibronectin-1 were analyzed by qRT-PCR. Data are expressed as means ± SEM. The experiment was repeated three times. A one-way ANOVA was used for the comparison among multiple groups, followed by a Bonferroni's post hoc test in (A)–(D) and (H). $p < 0.05$ was considered as statistically significant.

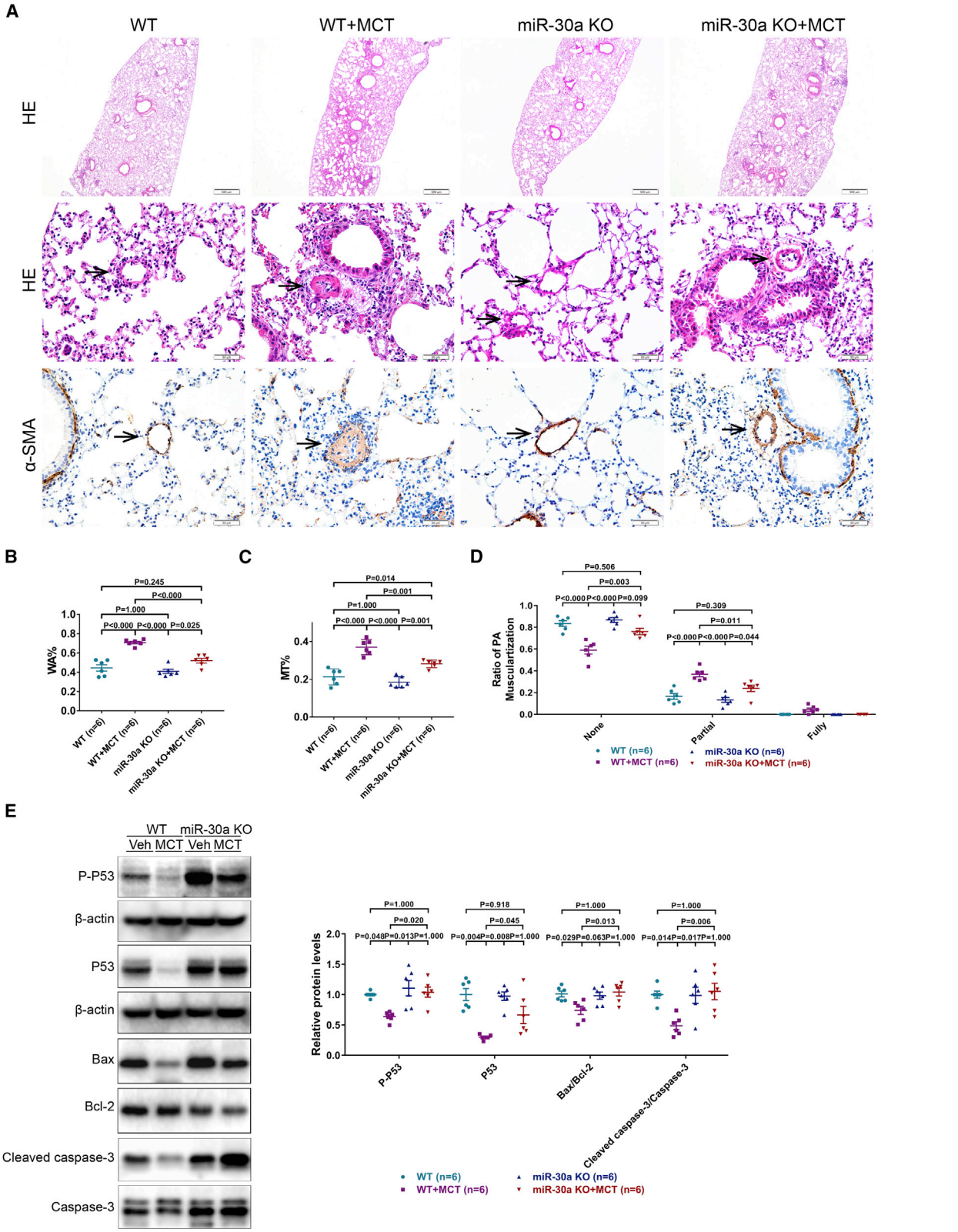

(legend on next page)

we verified that the expression of P53 could be restored by the inhibition of miR-30a in PAs in three animal experiments. *In vitro*, miR-30a could regulate the expression of P53 in PASMCs. Additionally, we found that inhibition of P53 reduced the beneficial effects of miR-30a antagomir. These data suggest that the miR-30a/P53 axis is a therapeutic target for PAH. In spite of the apoptosis pathways, miR-30a may also regulate other aspects of genes, including proliferation, inflammation, and fibrosis, which remains to be explored. In addition, the pathological phenotype of PAH seems to be triggered by multiple cells, such as PASMCs, PAECs, and fibroblasts. Researchers have observed that P53 is expressed at completely opposite levels in PASMCs and PAECs.[16] Our findings clarified the role of the miR-30a/P53 axis in PAs (mainly consisting of PASMCs) of animals and PASMCs cultivated *in vitro*. It is worth testing how this pathogenic mechanism occurs in PAECs and fibroblasts of PAH.

The regulatory mechanism of miRNAs is a complex process in which multiple factors interact.[5] Although some differences in pathology were observed, the Su5416/hypoxia-induced and the MCT-induced PAH models showed a gradual progression of PAH, accompanied by an increase of HIF-1α.[32] The rapid nuclear accumulation of HIF-1α in PASMCs regulates metabolism, proliferation, apoptosis, and other pathways involved in vascular remodeling.[15] In our previous study, we confirmed that HIF-1α regulated miR-30a in cardiomyocytes after hypoxia.[14] This regulatory mechanism may be a reasonable explanation for the same increase of miR-30a in our findings. Moreover, our findings suggested that the high miR-30a levels in the serum may be derived from PASMCs, as the miR-30a levels were increased in both PAs of PAH animals and in PASMCs after hypoxia. However, it still remains to be explored whether miR-30a originating from other cells could be transported to PASMCs. As mediators of intercellular communication, exosomes transfer various bioactive molecules, especially miRNAs, to adjacent or distant target cells to modulate cellular function.[33] Recently, exosomes have been found to retain the original characteristics of their parental cells,[34] while our previous studies have shown that hypoxic cardiomyocytes enrich miR-30a into exosomes.[14] Therefore, it is promising to study other sources of miR-30a by tracing the characteristics of exosomes that are derived from their parental cells.

miRNAs, as natural antisense nucleotides, have great potential in disease targeted treatments, and exhibit lower immune responses and toxicity compared to plasmid DNA-based gene therapy and protein-based drug molecules.[35] Recently, several miRNA modulators including miR-34 and miR-122 have entered different stages of clinical trials.[36,37] Pulmonary and transpulmonary drug delivery have unique functions and advantages for the treatment of pulmonary diseases, including immediate access to the airways and the lung for local treatment, rapid drug onset, low risk of infections, and painless and comfortable application.[38] In fact, triptorelin and iloprost have been repurposed for aerosol therapy of PAH, but both of them are capable of alleviating symptoms by dilating pulmonary vessels rather than reversing vascular remodeling,[39] and, as a result, their therapeutic efficacy is limited. In our study, a novel delivery system, IT-L, which requires a smaller dose of drugs, has lower immunotoxicity, and has higher lung expression levels than do intravenous and abdominal administration,[19] was used to evaluate the treatment effect in PAH mice. Throughout the course of the experiment, we used the lowest dose recommended by the manufacturer's instructions to treat animals weekly. To our satisfaction, we found that this therapeutic strategy performed well in decreasing RVSP, RV hypertrophy, and vascular remodeling, as well as clearly elevating the expression of target gene. Our findings, to some extent, confirmed the feasibility of using miR-30a therapy for PAH and described an effective delivery strategy.

In summary, we demonstrate that inhibition of miR-30a could ameliorate experimental PAH through the miR-30a/P53 signaling pathway, and the IT-L delivery strategy shows good therapeutic outcomes, which together provide a novel and promising approach for the treatment of PAH.

MATERIALS AND METHODS

Human subjects and ethics statement

In total, 81 PAH patients and 49 healthy controls between 2019 and 2020 at the Wuhan Union Hospital were selected for the study. All of the PAH patients, including idiopathic PAH, valvular diseases, and pulmonary thromboembolism, were diagnosed with pulmonary artery systolic blood pressure higher than 30 mmHg by echocardiography, as previously described.[40,41] Patients who had severe cardiopulmonary diseases, such as cardiomyopathy, hypertension, myocardial infarction, and pericardial diseases, were excluded from the study. All of the patients did not receive any surgery or treatment before informed consent was obtained. Venous blood samples (5 mL) were collected from individual subjects. All serum samples were centrifuged at room temperature for 30 min at 1,500 × *g* and then stored at −80°C for analysis. All experimental procedures on animals were performed strictly in accordance with the National Institutes of Health *Guidelines for the Care and Use of Laboratory Animals*. Animal experiments and human subjects were approved by the

Figure 5. Knockout of miR-30a enhances apoptosis of PAs to reverse vascular remodeling in the MCT mouse model

(A) Representative images of PAs are provided from each group. Lung sections were stained with H&E (upper and middle panels) and α-SMA (lower panel). Scale bars, 500 μm (upper panel) and 50 μm (middle and lower panels). (B) WA% of vessels. (C) MT% of vessels. (D) Percentage of muscularized vessels. Each vessel was classified as either nonmuscular, partially muscular, or fully muscular as previously described. (E) Protein expression levels of P-P53, P53, Bax/Bcl-2, and cleaved caspase-3/caspase-3 of PAs. All of the PAs (15–25 vessels per mouse, 25–75 μm in diameter) were calculated blinded to the source of the group. Data are expressed as means ± SEM. The experiment was repeated three times. A one-way ANOVA was used for the comparison among multiple groups, followed by a Bonferroni's post hoc test in (B)–(D) and Bax/Bcl-2 and cleaved caspase-3/caspase-3 of (E). The nonparametric data were analyzed using a Kruskal-Wallis test in P-P53 and P53 of (E). $p < 0.05$ was considered as statistically significant.

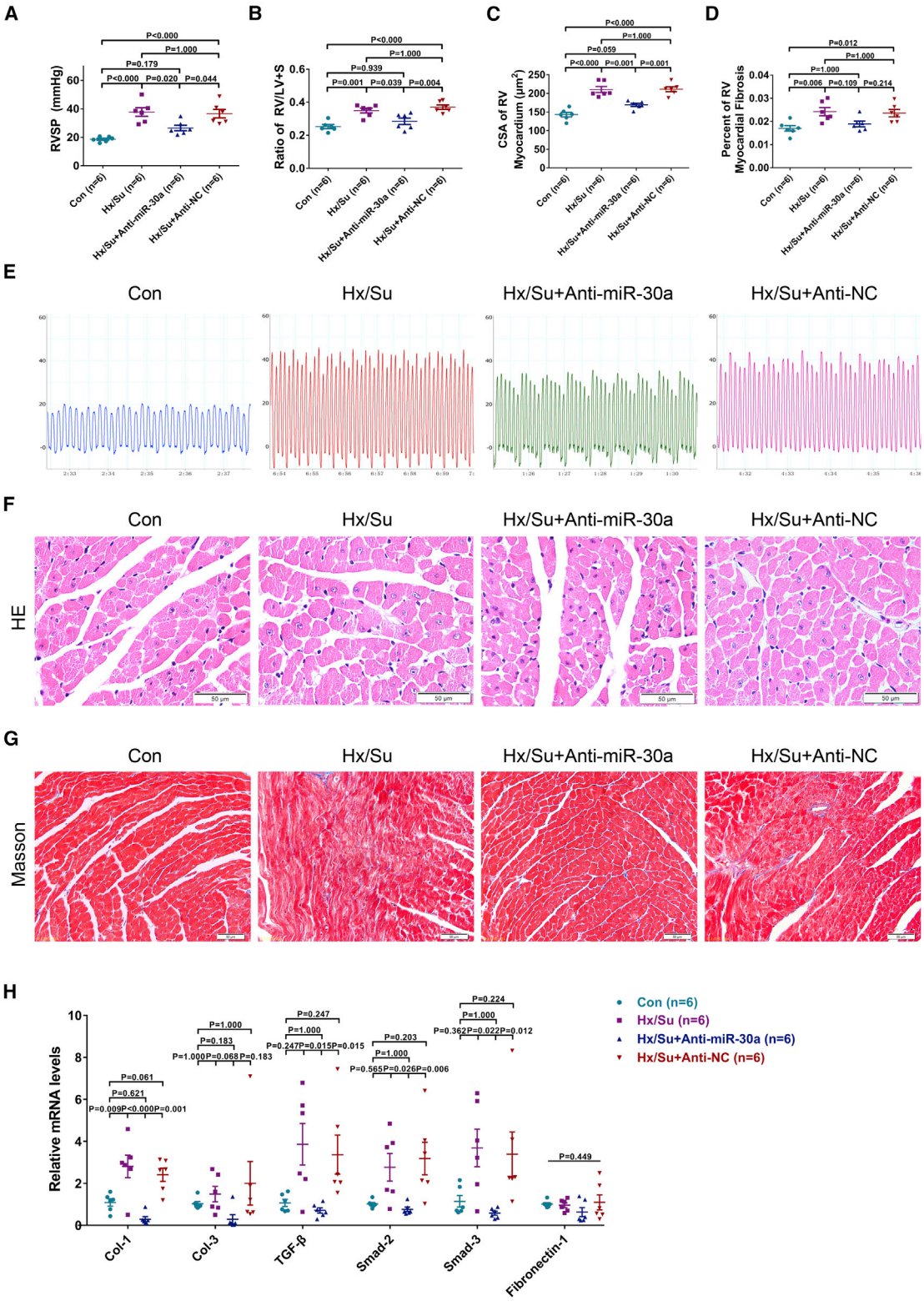

(legend on next page)

Institutional Animal Care and Use Committee at Tongji Medical College, Huazhong University of Science and Technology, and by the Ethics Committee of Tongji Medical College, Huazhong University of Science and Technology, respectively.

Cell culture, hypoxia treatment, and transfections

Human PASMCs were purchased from the American Type Culture Collection (ATCC, Manassas, VA, USA) and cultured in Dulbecco's modified Eagle's medium (DMEM, Thermo Scientific, Rockford, IL, USA) supplemented with 10% fetal bovine serum (FBS, Invitrogen, Carlsbad, CA, USA). For the normoxia-treated group, cells were maintained in 5% CO_2-95% mixed air (21% O_2) at 37°C, and the hypoxic group was cultured in 1% O_2 at 37°C for different time points.

To knockdown and overexpress miR-30a, the inhibitor and mimic of miR-30a, the inhibitor NC and mimic NC were purchased from RiboBio (Guangzhou, China). Cells were transfected using Lipofectamine 3000 reagent (Thermo Fisher Scientific, Rockford, IL, USA). All experiments were performed according to the manufacturer's instructions.

Su5416/hypoxia-induced pulmonary hypertension

miRNA-30a KO mice were obtained under license from Nanjing Biomedical Research Institute of Nanjing University (project no. XM001304). miR-30a KO mice or age-matched WT controls (strain C57BL/6, 8 weeks of age) were randomly divided into 4 groups: (1) a vehicle-normoxia-treated WT group (WT+Nor/Veh) (n = 10); (2) a Su5416-hypoxia-treated WT group (WT+Su/Hx) (n = 10); (3) a vehicle-normoxia-treated miR-30a$^{-/-}$ group (miR-30a KO+Nor/Veh) (n = 6); and (4) a Su5416-hypoxia-treated miRNA-30a$^{-/-}$ group (miR-30a KO+Su/Hx) (n = 8). The WT+Su/Hx and miR-30a KO+Su/Hx groups were injected subcutaneously with Su5416 (20 mg/kg, TargetMol, Boston, MA, USA) weekly, which was suspended in CMC (0.5% [w/v] carboxymethylcellulose sodium, 0.9% [w/v] sodium chloride, 0.4% [v/v] polysorbate 80, 0.9% [v/v] benzyl alcohol in deionized water) as previously described.[42] Then, the animals were exposed to chronic normobaric hypoxia (10% O_2) in a chamber for 21 days. The WT+Nor/Veh and miR-30a KO+Nor/Veh groups received only vehicle, and then the animals were kept in room air. At study termination, mice were anesthetized and sacrificed. A schematic of the experimental design is illustrated in Figure S1A.

MCT-induced pulmonary hypertension

Mice were randomly divided into four groups:1) a vehicle-treated WT group (WT) (n = 6); (2) an MCT-treated WT group (WT+MCT) (n = 6); (3) a vehicle-treated miRNA-30a$^{-/-}$ group (miR-30a KO) (n = 6); and (4) a MCT-treated miRNA-30a$^{-/-}$ group (miR-30a KO+MCT) (n = 6). MCT (Cayman Chemical, Ann Arbor, MI, USA) was dissolved in 0.1 N HCl, and the pH was adjusted to 7.4 with 0.1 N NaOH. Mice (8–10 weeks old) received weekly subcutaneous injections of MCT (600 mg/kg) for 4 consecutive weeks. All mice were sacrificed on day 28. A schematic of the experimental design is illustrated in Figure S1B.

IT-L

Adult male C57BL/6 mice (8–10 weeks old) were administered miRNA-30a antagomirs as described previously.[19] Mice were randomly divided into four groups: (1) a vehicle-normoxia-treated control group (Con) (n = 6); (2) a Su5416-hypoxia-treated group (Su/Hx) (n = 6); (3) a Su5416-hypoxia group treated with miR-30a antagomir (Su/Hx+anti-miR-30a) (n = 6); and (4) a Su5416-hypoxia group treated with negative control (Su/Hx+anti-NC) (n = 6).

Animals were operated on as described.[19] In short, the mice were anesthetized with ketamine (100 mg/kg) and placed in a 60° angle supine position on a platform. Then, the mice were intubated and ventilated using a standard rodent ventilator. The miR-30a antagomir/negative control (RioBio, Guangzhou, China) (5 nmol) was suspended in phosphate-buffered saline (PBS) (in a volume of 10 μL) in a liquid state according to the manufacturer's instructions. Then, the liquid was quickly injected into the catheter with a p20 micropipette. To minimize liquid remaining in the catheter or in the upper airways, a 1-mL syringe was attached to the end of the catheter to ventilate three times. After that, the mice were connected to a ventilator for at least 3 min before being returned to their cages. A schematic of the experimental design is illustrated in Figure S1C.

siRNA-P53 *in vivo* modifications and *in vivo* studies

Cholesterol-modified (RioBio, Guangzhou, China) siRNA-P53 was synthesized and used in the *in vivo* studies with the sequence 5′-GAATGAGGCCTTAGAGTTA-3′. The knockdown efficiency and specificity of all siRNAs were determined by qRT-PCR or western blotting. IT-L was used as before. Mice were randomly divided into five groups: (1) a vehicle-normoxia-treated control group (Con) (n = 6); (2) a Su5416-hypoxia-treated group (Su/Hx) (n = 10); (3) a Su5416-hypoxia group treated with miR-30a antagomir (anti-miR-30a) (n = 8); (4) a Su5416-hypoxia group treated with miR-30a antagomir and siRNA-P53 (anti-miR-30a+ siRNA-P53) (n = 8); and (5) a Su5416-hypoxia group treated with miR-30a antagomir and siRNA-NC (anti-miR-30a+ siRNA-NC) (n = 8). A schematic of the experimental design is illustrated in Figure S1D.

Figure 6. Intratracheal instillation of miR-30a antagomir reduces RVSP and RV hypertrophy in the Su5416/hypoxia mouse model

(A) Detection of RVSP by right cardiac catheterization. (B) RV hypertrophy measured by the weight ratio of RV/(LV+S). (C) Quantification of the CSA of RV cardiomyocytes. (D) Quantification of the RV fibrotic area. (E) Representative images of RVSP in the four groups. (F) Representative images of H&E staining of the RV cardiomyocytes in the four groups. Scale bars, 50 μm. (G) Representative images of Masson's trichrome staining of the RV in the four groups. Scale bars, 50 μm. (H) mRNA expression levels of Col-1, Col-3, TGF-β, Smad2, Smad3, and fibronectin-1 were analyzed by qRT-PCR. Data are expressed as means ± SEM. The experiment was repeated three times. A one-way ANOVA was used for the comparison among multiple groups, followed by a Bonferroni's post hoc test in (A)–(D) and Col-1 of (H). The nonparametric data were analyzed using Kruskal-Wallis test in Col-3, TGF-β, Smad2, Smad3, and fibronectin-1 of (H). $p < 0.05$ was considered as statistically significant.

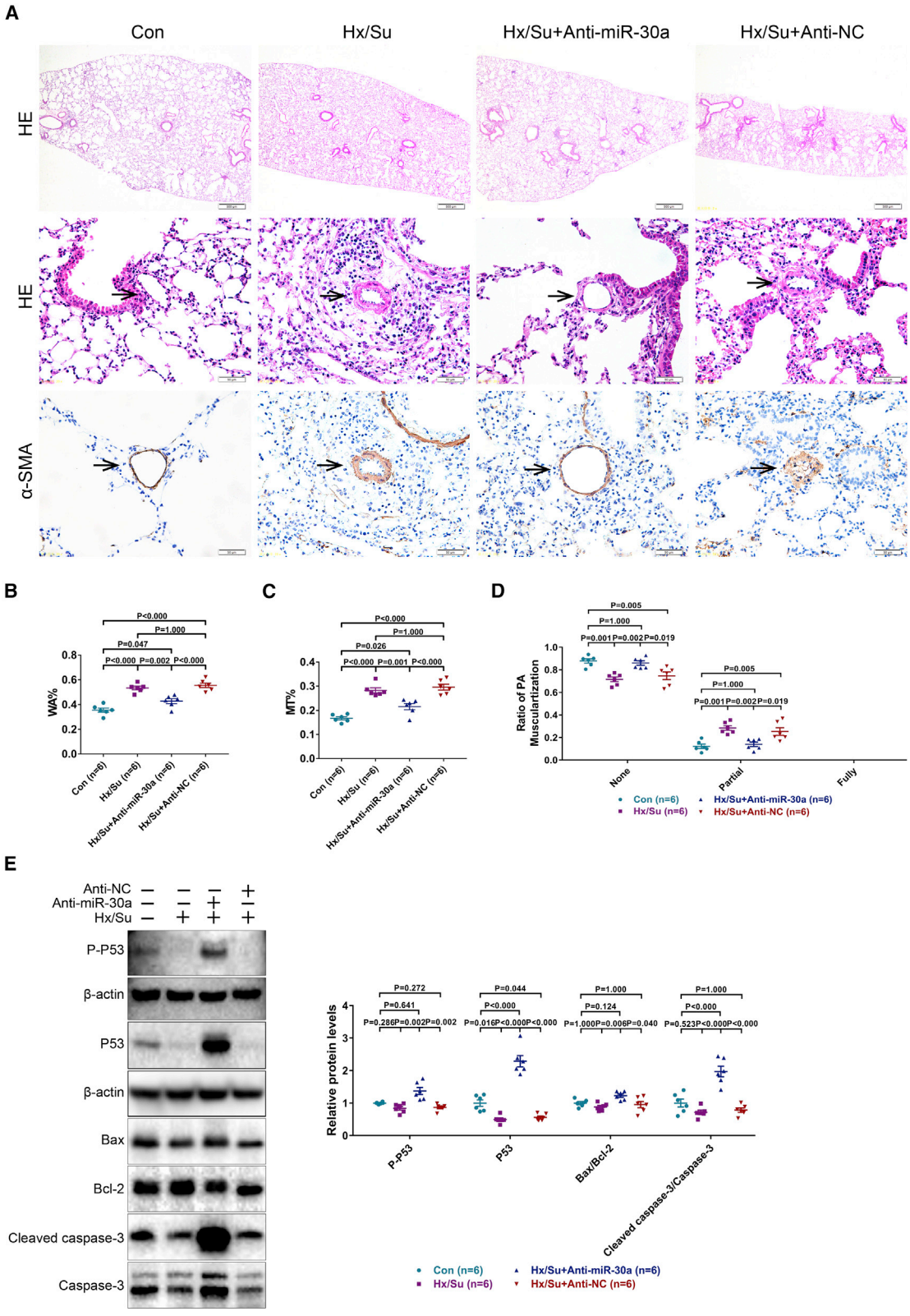

(legend on next page)

Hemodynamic measurements

Animals were anesthetized with ketamine (100 mg/kg). RVSP was measured using a closed-chest approach. Briefly, mice were first anesthetized with ketamine (100 mg/kg). The right neck skin was cut and the subcutaneous tissue and muscle were separated. Then, the external jugular vein was exposed and the adipose tissue on its surface was removed. The distal end of the external jugular vein was ligated with fine cotton thread. The external jugular vein with forceps was lifted, 1-mm opening was cut, and quickly inserted the catheter (SPR-839NR, Millar Instruments, Houston, TX, USA) was inserted quickly into the RV of the heart. The catheter was stabilized in the center of the RV for 1 min before recording ventricular waves with high amplitude using a polygraph system (LabChart 7.3.7; ADInstruments, Bella Vista, NSW, Australia). After the hemodynamic measurements, the Fulton index (RV/LV+S) was determined as the ratio of the ventricular wall weight to the left ventricle plus septum weight to evaluate RV hypertrophy.

Morphological assessment

Lung specimens and RV were washed with PBS through the pulmonary artery, fixed in 10% formalin, and embedded in paraffin as previously described.[42] The CSA and fibrotic area of the myocardium (%) were determined through H&E and Masson's trichrome staining. PA (25–75 μm diameter) remodeling was performed by H&E and α-smooth muscle actin (α-SMA). The MT% and WA% of vessels were calculated. To determine the degree of muscularization of vessels, each vessel was categorized as nonmuscular, partially muscular, or fully muscular according to the layers of SMCs in the vessels as previously described.[43] All of the analyses were performed by researchers who were blinded to the study conditions.

TUNEL assays

To detect apoptosis, a TUNEL assay (Roche Applied Science, Mannheim, Germany) was performed according to the manufacturer's instructions. Then, images of TUNEL assays were observed using laser confocal microscopy. The number of TUNEL-positive PASMCs was counted as the percentage from total PASMCs per vessel. The presented values are the means of 20–30 vessels per mouse.

Isolation of pulmonary arteries

The PAs were obtained as previously described.[16] In short, we dissected the whole lungs from the mouse, and then the intrapulmonary arteries were isolated from the whole lungs using a microscope. The adventitia of the PAs was dissected and the epithelium was destroyed with a cotton swab. At last, protein was extracted from the PAs for further study.

Western blotting

Proteins extracted from cultured cells and the pulmonary arteries of mice were quantified with bicinchoninic acid (BCA) protein assay kits (Thermo Scientific, Rockford, IL, USA). Equal amounts of protein were separated on 10% SDS-PAGE gel and transferred onto polyvinylidene fluoride (PVDF) membranes. The membranes were incubated for 2 h at 22°C–24°C in blocking buffer (0.1% Tween 20 in Tris-buffered saline [TBS] [TBST]) containing 5% nonfat dry milk powder. After blocking, the membranes were incubated overnight at 4°C with primary antibodies, including P53 (1:1,000, 2524S, Cell Signaling Technology), P-P53 (1:1,000, 9284S, Cell Signaling Technology), Bax (1:1,000, 50599-2-lg, Proteintech), β-actin (1:1,000, 60008-1-lg, Proteintech), Bcl-2 (1:500, 12789-1-AP, Proteintech), caspase-3 (1:1,000, 19677-1-AP, Proteintech), cleaved caspase-3 (1:1,000, 9661S, Cell Signaling Technology), CD31 (1:1,000, 77699T, Cell Signaling Technology), α-SMA (1:1,000, 14395-1-AP, Proteintech), HIF-1α (1:1,000, 36169, Cell Signaling Technology), and secondary antibodies (goat anti-mouse and anti-rabbit antibodies) were used at a dilution of 1:3,000. Proteins were visualized by the enhanced chemiluminescence (ECL) system (ECL western blotting detection kit, Thermo Scientific, Rockford, IL, USA). The densities of the bands were quantified by ImageJ software.

Quantitative RT-PCR (qRT-PCR) Analysis

Total RNAs were extracted from different tissues, cells, or serum using TRIzol (Vazyme, Nanjing, China) and a commercial miRNeasy serum/plasma kit (QIAGEN, #217184) according to the manufacturer's instructions. RNAs were reverse transcribed into cDNA using the PrimeScript RT reagent kit (Vazyme, Nanjing, China) following the manufacturer's protocol. qRT-PCR was performed using SYBR Green master mix (Vazyme, Nanjing, China) with the 7500 Fast real-time PCR system from Applied Biosystems (Bio-Rad, Hercules, CA, USA). qRT-PCR primers of mature miRNAs (catalog nos. MQPS0000940, MQPS0000942, MQPS0000945, MQPS0000947, and MQPS0000949) were purchased from RioBio (Guangzhou, China). The sequences of the primers are shown in Table S1. Normalization of miR-30a levels in the serum was performed using synthetic *C. elegans* miRNA cel-miR-39 (250 fmol, RioBio, Guangzhou, China). Normalization of miR-30a levels in the tissues/cells was performed using U6. The relative expression level of miR-30a was analyzed by qRT-PCR, with levels normalized to cel-miR-39 or U6 using the $2^{-\Delta\Delta CT}$ method.

Quantification of microRNA expression using qRT-PCR

The TaqMan miRNA assay (Thermo Scientific, USA, #4427957) was used to determine the copy numbers of miR-30a in the serum samples. qRT-PCR standard curve was generated using serial dilutions

Figure 7. Intratracheal instillation of miR-30a antagomir increases apoptosis of PAs to mitigate vascular remodeling in the Su5416/hypoxia mouse model

(A) Representative images of PAs are provided from each group. Lung sections were stained with H&E (upper and middle panels) and α-SMA (lower panel). Scale bars, 500 μm (upper panel) and 50 μm (middle and lower panels). (B) WA% of vessels. (C) MT% of vessels. (D) Percentage of muscularized vessels. Each vessel was classified as either nonmuscular, partially muscular, or fully muscular as previously. (E) Protein expression levels of P-P53, P53, *Bax*/Bcl-2, and cleaved caspase-3/caspase-3 of PAs. All of the PAs (15–25 vessels per mouse, 25–75 μm in diameter) were calculated blinded to the source of group. Data are expressed as means ± SEM. The experiment was repeated three times. A one-way ANOVA was used for the comparison among multiple groups, followed by a Bonferroni's post hoc test in (B)–(D) and P53, Bax/Bcl-2, and cleaved caspase-3/caspase-3 of (E). The nonparametric data were analyzed using a Kruskal-Wallis test in P-P53 of (E). $p < 0.05$ was considered as statistically significant.

of cel-miR-39 (100 pM, 10 pM, 1 pM, 100 fM, 10 fM, 1 fM). The cycle threshold (Ct) values of cel-miR-39 of serial dilutions from each reaction and corresponding copy numbers were determined. The formula for normalization between samples is as follows: normalized amount of miR-30a in sample X = (pre-normalized amount of the miR-30a in sample X) × (the amount of cel-miR-39 in the reference sample/the amount of cel-miR-39 in sample X).

Statistical analysis

Data are presented as means ± SEM. A Student's t test (for comparison between two groups) and one-way analysis of variance (ANOVA) using Bonferroni's method (for comparison of multiple groups) were used for the statistical analyses when the variance was homogeneous. The nonparametric data were analyzed using a Kruskal-Wallis test. The serum levels of miR-30a in the PAH patients and healthy controls were compared by a Mann-Whitney U test. The calculation was analyzed with the statistical program SPSS version 23.0 (IBM, Armonk, NY, USA). $p < 0.05$ was considered as statistically significant.

SUPPLEMENTAL INFORMATION

Supplemental information can be found online at https://doi.org/10.1016/j.omtn.2021.09.007.

ACKNOWLEDGMENTS

This work was supported by the National Natural Science Foundation of China (grant nos. 82070522, 81974055, 81770366, 81900401, and 81900459).

AUTHOR CONTRIBUTIONS

W.M. and Z.B. carried out the animal experiments. Y.D. and C.L. participated in analyzing the data. Z.Z., M.L., and Z.Q. conceived and designed the experiments. Y.L. drafted the manuscript. X.C. and X.S. contributed to scientific discussions. D.S. collected the human samples. Y.Z. and Y.P. supported calcification analysis. All authors read and approved the final version of the paper.

DECLARATION OF INTERESTS

The authors declare no competing interests.

REFERENCES

1. Thenappan, T., Ormiston, M.L., Ryan, J.J., and Archer, S.L. (2018). Pulmonary arterial hypertension: Pathogenesis and clinical management. BMJ *360*, j5492.
2. Hoeper, M.M., McLaughlin, V.V., Dalaan, A.M., Satoh, T., and Galiè, N. (2016). Treatment of pulmonary hypertension. Lancet Respir. Med. *4*, 323–336.
3. Crnkovic, S., Marsh, L.M., El Agha, E., Voswinckel, R., Ghanim, B., Klepetko, W., Stacher-Priehse, E., Olschewski, H., Bloch, W., Bellusci, S., et al. (2018). Resident cell lineages are preserved in pulmonary vascular remodeling. J. Pathol. *244*, 485–498.
4. Steffes, L.C., Froistad, A.A., Andruska, A., Boehm, M., McGlynn, M., Zhang, F., Zhang, W., Hou, D., Tian, X., Miquerol, L., et al. (2020). A Notch3-marked subpopulation of vascular smooth muscle cells is the cell of origin for occlusive pulmonary vascular lesions. Circulation *142*, 1545–1561.
5. Bartel, D.P. (2018). Metazoan microRNAs. Cell *173*, 20–51.
6. Bienertova-Vasku, J., Novak, J., and Vasku, A. (2015). MicroRNAs in pulmonary arterial hypertension: Pathogenesis, diagnosis and treatment. J. Am. Soc. Hypertens. *9*, 221–234.
7. Hong, Z., Chen, K.H., DasGupta, A., Potus, F., Dunham-Snary, K., Bonnet, S., Tian, L., Fu, J., Breuils-Bonnet, S., Provencher, S., et al. (2017). MicroRNA-138 and microRNA-25 down-regulate mitochondrial calcium uniporter, causing the pulmonary arterial hypertension cancer phenotype. Am. J. Respir. Crit. Care Med. *195*, 515–529.
8. Mellios, N., Huang, H.S., Grigorenko, A., Rogaev, E., and Akbarian, S. (2008). A set of differentially expressed miRNAs, including miR-30a-5p, act as post-transcriptional inhibitors of BDNF in prefrontal cortex. Hum. Mol. Genet. *17*, 3030–3042.
9. Jiang, L.H., Zhang, H.D., and Tang, J.H. (2018). miR-30a: A novel biomarker and potential therapeutic target for cancer. J. Oncol. *2018*, 5167829.
10. Li, W.F., Dai, H., Ou, Q., Zuo, G.Q., and Liu, C.A. (2016). Overexpression of microRNA-30a-5p inhibits liver cancer cell proliferation and induces apoptosis by targeting MTDH/PTEN/AKT pathway. Tumour Biol. *37*, 5885–5895.
11. Thompson, A.A.R., and Lawrie, A. (2017). Targeting vascular remodeling to treat pulmonary arterial hypertension. Trends Mol. Med. *23*, 31–45.
12. Rothman, A., Restrepo, H., Sarukhanov, V., Evans, W.N., Wiencek, R.G., Jr., Williams, R., Hamburger, N., Anderson, K., Balsara, J., and Mann, D. (2017). Assessment of microRNA and gene dysregulation in pulmonary hypertension by endoarterial biopsy. Pulm. Circ. *7*, 455–464.
13. Tan, H., Yao, H., Lie, Z., Chen, G., Lin, S., and Zhang, Y. (2019). MicroRNA-30a-5p promotes proliferation and inhibits apoptosis of human pulmonary artery endothelial cells under hypoxia by targeting YKL-40. Mol. Med. Rep. *20*, 236–244.
14. Yang, Y., Li, Y., Chen, X., Cheng, X., Liao, Y., and Yu, X. (2016). Exosomal transfer of miR-30a between cardiomyocytes regulates autophagy after hypoxia. J. Mol. Med. (Berl.) *94*, 711–724.
15. Shimoda, L.A., and Semenza, G.L. (2011). HIF and the lung: Role of hypoxia-inducible factors in pulmonary development and disease. Am. J. Respir. Crit. Care Med. *183*, 152–156.
16. Wang, Z., Yang, K., Zheng, Q., Zhang, C., Tang, H., Babicheva, A., Jiang, Q., Li, M., Chen, Y., Carr, S.G., et al. (2019). Divergent changes of p53 in pulmonary arterial endothelial and smooth muscle cells involved in the development of pulmonary hypertension. Am. J. Physiol. Lung Cell. Mol. Physiol. *316*, L216–L228.
17. Zhang, C., Liao, P., Liang, R., Zheng, X., and Jian, J. (2019). Epigallocatechin gallate prevents mitochondrial impairment and cell apoptosis by regulating miR-30a/p53 axis. Phytomedicine *61*, 152845.
18. Spiekerkoetter, E., Kawut, S.M., and de Jesus Perez, V.A. (2019). New and emerging therapies for pulmonary arterial hypertension. Annu. Rev. Med. *70*, 45–59.
19. Schlosser, K., Taha, M., and Stewart, D.J. (2018). Systematic assessment of strategies for lung-targeted delivery of microRNA mimics. Theranostics *8*, 1213–1226.
20. Meloche, J., Pflieger, A., Vaillancourt, M., Graydon, C., Provencher, S., and Bonnet, S. (2014). miRNAs in PAH: Biomarker, therapeutic target or both? Drug Discov. Today *19*, 1264–1269.
21. Paulin, R., Courboulin, A., Barrier, M., and Bonnet, S. (2011). From oncoproteins/tumor suppressors to microRNAs, the newest therapeutic targets for pulmonary arterial hypertension. J. Mol. Med. (Berl.) *89*, 1089–1101.
22. Cheng, X., Wang, Y., and Du, L. (2019). Epigenetic modulation in the initiation and progression of pulmonary hypertension. Hypertension *74*, 733–739.
23. Mao, L., Liu, S., Hu, L., Jia, L., Wang, H., Guo, M., Chen, C., Liu, Y., and Xu, L. (2018). miR-30 family: A promising regulator in development and disease. BioMed Res. Int. *2018*, 9623412.
24. Sheikh, A.Q., Misra, A., Rosas, I.O., Adams, R.H., and Greif, D.M. (2015). Smooth muscle cell progenitors are primed to muscularize in pulmonary hypertension. Sci. Transl. Med. *7*, 308ra159.
25. Kruiswijk, F., Labuschagne, C.F., and Vousden, K.H. (2015). p53 in survival, death and metabolic health: A lifeguard with a licence to kill. Nat. Rev. Mol. Cell Biol. *16*, 393–405.
26. Chipuk, J.E., and Green, D.R. (2006). Dissecting p53-dependent apoptosis. Cell Death Differ. *13*, 994–1002.
27. Estaquier, J., Vallette, F., Vayssiere, J.L., and Mignotte, B. (2012). The mitochondrial pathways of apoptosis. Adv. Exp. Med. Biol. *942*, 157–183.

28. Garcia, P.B., and Attardi, L.D. (2014). Illuminating p53 function in cancer with genetically engineered mouse models. Semin. Cell Dev. Biol. *27*, 74–85.

29. Rao, F., Cha, J., Xu, J., Xu, R., Vandiver, M.S., Tyagi, R., Tokhunts, R., Koldobskiy, M.A., Fu, C., Barrow, R., et al. (2020). Inositol pyrophosphates mediate the DNA-PK/ATM-p53 cell death pathway by regulating CK2 phosphorylation of Tti1/Tel2. Mol. Cell *79*, 702.

30. Wei, X.W., Yuan, J.M., Huang, W.Y., Chen, N.Y., Li, X.J., Pan, C.X., Mo, D.L., and Su, G.F. (2020). 2-Styryl-4-aminoquinazoline derivatives as potent DNA-cleavage, p53-activation and in vivo effective anticancer agents. Eur. J. Med. Chem. *186*, 111851.

31. Sutendra, G., and Michelakis, E.D. (2014). The metabolic basis of pulmonary arterial hypertension. Cell Metab. *19*, 558–573.

32. Lai, Y.L., and Law, T.C. (2004). Chronic hypoxia- and monocrotaline-induced elevation of hypoxia-inducible factor-1α levels and pulmonary hypertension. J. Biomed. Sci. *11*, 315–321.

33. Hu, W., Liu, C., Bi, Z.Y., Zhou, Q., Zhang, H., Li, L.L., Zhang, J., Zhu, W., Song, Y.Y., Zhang, F., et al. (2020). Comprehensive landscape of extracellular vesicle-derived RNAs in cancer initiation, progression, metastasis and cancer immunology. Mol. Cancer *19*, 102.

34. Nam, G.H., Choi, Y., Kim, G.B., Kim, S., Kim, S.A., and Kim, I.S. (2020). Emerging prospects of exosomes for cancer treatment: From conventional therapy to immunotherapy. Adv. Mater. *32*, e2002440.

35. Chen, Y., Gao, D.Y., and Huang, L. (2015). In vivo delivery of miRNAs for cancer therapy: Challenges and strategies. Adv. Drug Deliv. Rev. *81*, 128–141.

36. Bouchie, A. (2013). First microRNA mimic enters clinic. Nat. Biotechnol. *31*, 577.

37. Janssen, H.L., Reesink, H.W., Lawitz, E.J., Zeuzem, S., Rodriguez-Torres, M., Patel, K., van der Meer, A.J., Patick, A.K., Chen, A., Zhou, Y., et al. (2013). Treatment of HCV infection by targeting microRNA. N. Engl. J. Med. *368*, 1685–1694.

38. Gessler, T. (2018). Inhalation of repurposed drugs to treat pulmonary hypertension. Adv. Drug Deliv. Rev. *133*, 34–44.

39. Galiè, N., Humbert, M., Vachiery, J.L., Gibbs, S., Lang, I., Torbicki, A., Simonneau, G., Peacock, A., Vonk Noordegraaf, A., Beghetti, M., et al. (2015). 2015 ESC/ERS Guidelines for the diagnosis and treatment of pulmonary hypertension: The Joint Task Force for the Diagnosis and Treatment of Pulmonary Hypertension of the European Society of Cardiology (ESC) and the European Respiratory Society (ERS): Endorsed by: Association for European Paediatric and Congenital Cardiology (AEPC), International Society for Heart and Lung Transplantation (ISHLT). Eur. Respir. J. *46*, 903–975.

40. Habib, G., and Torbicki, A. (2010). The role of echocardiography in the diagnosis and management of patients with pulmonary hypertension. Eur. Respir. Rev. *19*, 288–299.

41. Ou, M., Zhang, C., Chen, J., Zhao, S., Cui, S., and Tu, J. (2020). Overexpression of microRNA-340-5p inhibits pulmonary arterial hypertension induced by APE by downregulating IL-1β and IL-6. Mol. Ther. Nucleic Acids *21*, 542–554.

42. Ciuclan, L., Bonneau, O., Hussey, M., Duggan, N., Holmes, A.M., Good, R., Stringer, R., Jones, P., Morrell, N.W., Jarai, G., et al. (2011). A novel murine model of severe pulmonary arterial hypertension. Am. J. Respir. Crit. Care Med. *184*, 1171–1182.

43. Mouraret, N., Marcos, E., Abid, S., Gary-Bobo, G., Saker, M., Houssaini, A., Dubois-Rande, J.L., Boyer, L., Boczkowski, J., Derumeaux, G., et al. (2013). Activation of lung p53 by Nutlin-3a prevents and reverses experimental pulmonary hypertension. Circulation *127*, 1664–1676.